Multicompartment Vesicles: A Key Intermediate Structure in Polymerization-Induced Self-Assembly of Graft Copolymers

Djallal Ikkene, Ana Andreea Arteni, Claire Boulogne, Jean-Luc Six, Khalid Ferji

Multi-Compartment Vesicle: A key Intermediate Structure in Polymerization Induced-Self-Assembly of Graft Copolymers

Djallal Ikkene,[a] Ana Andreea Arteni,[b] Claire Boulogne,[b] Jean-Luc Six,[a] and Khalid Ferji[a]*

[a] CNRS, LCPM, F-54000, Université de Lorraine 1 rue Grandville, Nancy 54001, France

[b] Institute for Integrative Biology of the Cell (I2BC), Université Paris-Saclay, CEA, CNRS CRYOEM-Gif, 91198, Gif-sur-Yvette, France

Corresponding author:

khalid.ferji@univ-lorraine.fr

KEYWORDS**:** Photo RAFT PISA; suspension; nanocarrier; cell model; glycopolymer; amphiphilic.

ABSTRACT.

The morphology evolution of graft copolymer-based nano-objects was monitored by light scattering and electron microscopy during their formulation in water by photo-mediated reversible addition-fragmentation chain transfer mediated polymerization induced self-assembly. Copolymers models composed of dextran backbone bearing poly(2-hydroxypropyl methacrylate) grafts of two degrees of polymerization (X) were used. At full monomers conversion, unilamellar vesicle (ULV) and large compound nano-objects (LCN) were formed when targeting X=100 and 500 respectively. For X=100, sphere, worm then jellyfish were progressively observed before forming ULV. For X=500, electron cryotomography revealed an unprecedented intermediate morphology formed from the onset of self-assembly, called multi-compartment vesicle (MCV), that fused to form LCN. The formation of MCV was attributed to a local phase separation between dextran and the residual HPMA inducing appearance of multiple hydrophilic cores.

INTRODUCTION.

Reversible addition-fragmentation chain transfer mediated polymerization induced self-assembly (RAFT PISA)[1-2] in aqueous phase is a straightforward platform technology developed to produce polymeric nano-object directly in water at high solids concentration.[3-5] Namely, aqueous RAFT PISA is based on the chain extension of a hydrophilic stabilizer by suitable monomers that form hydrophobic polymers, resulting in a progressive formation of amphiphilic copolymers that subsequently self-assemble *in-situ* into nano-objects.[6-14] Aqueous RAFT PISA has been extensively conducted for amphiphilic diblock copolymers in emulsion[15-18] and dispersion[19-23] media. Spherical micelle and latex are the predominant morphologies reported in the former, while a large set of advanced morphologies are produced in the latter including spherical/worm-like micelles, vesicles, framboidal and tubular vesicles as well as lamellae.

In PISA, morphology diagrams[24-27] have been typically constructed to easily target pure nano-objects morphology and to avoid the formation of undesirable mixture of morphologies. They were depicted from the morphology at full monomers conversion by varying both the core-forming polymer degree of polymerization and the solids concentration. However, these diagrams are not suited to investigate the mechanistic route leading to the desired morphology. *In-situ* monitoring of the morphology at progressive monomer conversion is an elegant pathway for this aim, since it allows trapping intermediate structures involved in the formation of the final targeted nano-object.[3-4, 28-35] Using this methodology, 'Jellyfish' morphology [3] has been identified as a key intermediate structure for worm-like micelle to vesicle transition by using poly(glycerol monomethacrylate)-*b*-poly(2-hydroxypropyl meth-acrylate) (PGMA-*b*-PHPMA) as copolymers models. Recently, the formation of tubular polymersomes in case of diblock copolymers was explained by a progressive vesicle-vesicle fusion pathway.[20, 36]

Graft copolymers, composed of a polymeric backbone carrying several polymeric grafts, are particularly interesting due to their architecture leading to specific physico-chemical properties that could differ from those of linear block copolymers.[37-38] However, as far as we are aware, reports on PISA of

graft copolymers are extremely limited.[39-42] Recently, our group reported a series of investigations on the formulation of graft copolymers-based nano-objects using a photo-mediated RAFT PISA (photo-RAFT PISA).[40-42] Copolymers used (Dex-g^{12}-PHPMA$_X$) were composed of dextran as hydrophilic backbone bearing on average 12 poly(2-hydroxypropyl methacrylate) (PHPMA$_X$) grafts of various degree of polymerization -$\overline{X_n}$- (noted X for simplicity). Our investigations revealed that such system form various morphologies depending on the grafts size.[42] At full monomers conversion, copolymers of short grafts (X=100) formed unilamellar vesicles (ULV) of thin membrane that became progressively thicker for intermediate degree of polymerization (X= 200 and 300). On the other hand, mixture of large compound nano-object (LCN) of spherical and cylindrical morphologies[41-42] were strangely observed when targeting higher grafts degree of polymerization (X $\geq$ 400). The appearance of cylinder-like nano-objects beyond ULVs contrasts the theoretical prediction of the packing parameter theory,[43] which assumes the formation of cylinders before vesicles when increasing the volume fraction of the hydrophobic part. One a likely explanation would be that LCNs result from a cooperative ULV-ULV fusion as reported by others for diblock copolymers.[20, 36]

Here, we used our model system (Dex-g^{12}-PHPMA$_X$) to assess whether fusion of ULVs causes formation of LCNs. A macromolecular chain transfer agent (DexCTA$_{12}$) based on dextran ($\overline{M_n}$=32000 g/mol, Đ=1.4), containing on average 12 photosensitive trithiocarbonate-type groups (CTA) per dextran chain, was prepared as we previously reported [44] and used as hydrophilic stabilizer in photo-RAFT PISA of 2-hydroxypropyl methacrylate (HPMA) in water under visible light (λ_{max}=405nm, max 60 mW/cm^2) (**Scheme 1**). Synthesis was performed at room temperature to avoid nano-objects morphology evolution with temperature.[41] Short (X=100 for PISA1) and large (X=500 for PISA2) PHPMA grafts were targeted to investigate respectively the morphology evolution toward and beyond the vesicular morphology previously observed by us at X=100.[42] Due to the rapid polymerization rate of photo-RAFT PISA, less than 30 min to achieve higher monomer conversion (99%), aliquots were extracted periodically at least

every 1 min. The morphology of nano-objects formed was carefully monitored at progressive monomer conversion using dynamic light scattering (DLS) and (cryo) transmission electron microscopy (cryo)TEM.

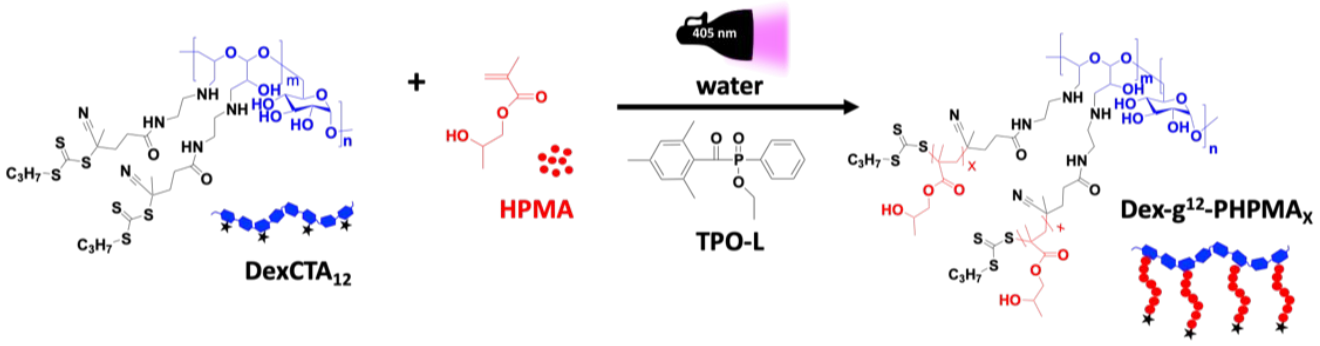

Scheme 1. Nano-objects of Dex-g^{12}-PHPMA$_X$ prepared by aqueous photo-RAFT PISA of HPMA from a dextran-based macromolecular chain transfer agent (DexCTA$_{12}$) in the presence of TPO-L as photo-initiator. The chemical structures of DexCTA$_{12}$ and Dex-g^{12}-PHPMA$_X$ are simplified for clarity.

MATERIALS AND METHODS

Materials

Chemical reagents.

Dextran ($\overline{M_n}$=32000 g mol^{-1}, Đ=1.4) and poly(ethylene oxide) ($\overline{M_n}$=5000 g mol^{-1}) were purchased from Sigma-Aldrich (Merck). 2-hydroxypropyl methacrylate (HPMA) (98%) was purchased from ABCR and passed through a silica gel column before use. 4-(propylthiocarbonothioylthio)-4-cyanopentanoic acid was synthesized as we reported previously.[40, 45] Ethyl (2, 4, 6-trimethylbenzoyl) phenylphosphinate (TPO-L) was purchased from fluorochem and used without purification.

Synthesis of the macromolecular chain transfer agent, DexCTA$_{12}$.

The macromolecular chain transfer agent containing an average of 12 CTA groups per dextran chain was synthesized through a multistep strategy as we previously reported.[44]

In-situ monitoring of nano-objects formulation via photo-RAFT PISA.[42]

In a typical reaction for the synthesis of Dex-g[12]-PHPMA$_X$ (X=100 and 500) at 10% solids concentration: DexCTA$_{12}$ and HPMA were dissolved in milli-Q. The solution was purged with nitrogen for 10 minutes, then TPO-L was added to the flask vial under nitrogen. The reaction medium was irradiated under stirring with a visible LED lamp (λ_{max}= 405 nm, max 60 mW cm^{-2}) at 20 °C. Aliquots were extracted periodically and characterized by ^{1}H NMR, dynamic light scattering (DLS) and (cryo) transmission electron microscopy (cryo)TEM. The experimental conditions used for each kinetic are summarized in the **Table S1**.

Characterization methods

^{1}H NMR spectroscopy: ^{1}H NMR analysis was conducted on a Brüker Advance 300 MHz NMR spectrometer and DMSO-d_6 was used as solvent.

Size exclusion chromatography (SEC): The number-average molar mass ($\overline{M_n}$) and the dispersity (Đ) were determined by SEC in DMSO/$NaNO_3$ (8.5 g L^{-1}) at 70 °C at 0.7 mL min^{-1}. The refractive indexes increment (dn/dc) of DexCTA$_{12}$ and Dex-g[12]-PHPMA$_X$ were used as previously estimated.[44] Experiments were performed using a Shimadzu SEC device equipped with an HPLC pump (LC 20AD, Shimadzu), a degasser AF (DGU – 20A3R, Shimadzu), three PL gel columns (100000, 1000, and 100 Å), a multi-angle laser light scattering (MALLS) detector (Wyatt Technology, Mini Dawn, with a He–Ne light wavelength at 632.8 nm), a differential refractometer detector (RID 10A, Shimadzu), and a UV detector (SPD-20A, Shimadzu, 310 nm).

Dynamic Light Scattering (DLS): Hydrodynamic radius (R_H) and size distribution of nanoobjects were determined at 20°C using an ALV/CGS-3 compact goniometer system equipped with an ALV-7004

multiple tau digital correlator and a vertically-polarized He-Ne laser of 22 mW output power operating at wavelength λ = 632.8 nm. The autocorrelation functions were analyzed in terms of relaxation time (τ) distribution according to REPES routine. Measurements were done at angles θ varying from 20° to 150° corresponding to scattering wave vectors q ranging from $q = 4.6 \times 10^{-3}$ to 2.55×10^{-2} nm^{-1}. Z-average hydrodynamic radius (R_H) was estimated using the Stokes-Einstein relation (1), where D_0 is the diffusion coefficient, k_B is the Boltzmann constant, T is the experimental temperature (293 K) and η_s is the viscosity of the solvent (water).

$$R_H = \frac{k_B T}{3\pi \eta_s D_0} \quad (1)$$

Transmission electron microscopy (TEM): Samples were analyzed by conventional electron microscopy using the negative staining method. Three microliters of the nanoobjects suspension were deposited on an air glow-discharged carbon-coated grid for 1 minute. The excess of liquid was blotted, and the grid rinsed with 2 % w/v aqueous uranyl acetate. The grids were visualized at 100 kV with a Tecnai 12 Spirit transmission electron microscope (Thermo Fisher, New York NY, USA) equipped with a K2 Base 4k x 4k camera (Gatan, Pleasanton CA, USA). Magnification was at 4400, 6500 or 15000 X, corresponding to a pixel size at the level of the specimen of 0.83, 0.55 and 0.25 nm, respectively.

Cryogenic electron microscopy (CryoEM): Samples were prepared for CryoEM using a Vitrobot Mark IV. Three microliters of the nanoobjects suspension was deposited on airglow-discharged Quantifoil R2/2 grids. The sample was blotted for 4-5 seconds using force value 2, and frozen in liquid-nitrogen-cooled ethane. Grids were observed on a Tecnai 20 G2 (Thermo Fisher), equipped with a field emission gun and operated at 200 kV. Images were recorded on a K2 Summit camera (Gatan) at a magnification of 15,000 X at the level of the microscope (0.25 nm pixel size); defocus was between -1.5 and 3 µm. Data were recorded under low dose conditions (dose rate $\sim 20\ e^{-}/Å^2$).

Electron cryotomography (ECT): EM grids containing the sample were plunge-frozen in a liquid ethane using a Vitrobot Mark IV (FEI). The Vitrobot was set to 100% relative humidity at 20°C and blotting was done using BF 2, BT 6. Nano-gold particles, Protein A gold (from CMC, Uthecht, NL) were diluted 10 times in PBS buffer and mixed 1:1 with the sample just before blotting and plunge freezing. Plunge-frozen grids were subsequently loaded into Glacios autogrid cartridges (ThermoFisher). Cryo-ET was performed using a ThermoFisher Glacios microscope 200 kV X-FEG microscope at NanoImaging Core of Pasteur Institute. The microscope were equipped with a 4k x 4k Falcon3 camera (ThermoFisher) operated in electron counting mode. Magnifications was at 36.000, corresponding to pixel sizes of 4A. Once the areas of interest were identified and marked, anchor maps were used to revisit these locations and collect tilt-series in an automated fashion. Each tilt-series was collected from negative 60° to positive 60° with an increment of 2° using the low dose functions of tracking and focusing. The cumulative dose of each tilt-series was 120 e-/Å2. Once acquired, tilt-series were binned into 1k x 1k arrays before alignment and reconstruction into 3D tomograms with the IMOD software package.[46] Tilt series were aligned using gold fiducials while reconstructions were performed using WBP algorithm.

RESULTS AND DISCUSSION.

Figures 1A and 1B show the visual appearance of aliquots sampled at different time during PISA1 and PISA2, respectively. The monomers conversion was determined by ^{1}H NMR analysis (**Figure S1 and S2**). The kinetic study summarized in **Figures 1C and 1D** shows a similar behavior for both experiments (PISA1 and PISA2). A non-linear evolution of $\ln([M]_0/[M]_t)$ versus time that displays two-time domains is observed as typically reported in PISA of HPMA.[3, 40] Briefly, in the first domain (up to 3.5min for PISA1 and 5min for PISA2), the reaction medium remained homogeneous and monophasic revealing a modest growth of PHPMA grafts that resulted in the formation of water-soluble copolymers. The turbidity observed from 3.5min (PISA1) and 5min (PISA2), called onset of self-assembly time, indicates that PHPMA grafts have reached their water-soluble critical size (X=36 and X=105

respectively) and became hydrophobic. This led to the formation of amphiphilic copolymers that self-assembled *in situ* into nano-objects. The delay in turbidity observed in PISA2 (up to X=105) is explained by the presence of a large quantity of HPMA that maintains the solubility of the PHPMA grafts in the medium up to high degree of polymerization compared to X=36 observed in PISA1. In the second domain (from 3.5 to 9min for PISA1 and from 5 to 16min for PISA2) the dispersion became progressively heterogeneous and opaque involving an increase of the slop of the linear evolution of $\ln([M]_0/[M]_t)$ with time. This specific kinetic profile is attributed to the diffusion of residual HPMA monomers into nano-objects resulting in an increase of the local monomer concentration and thus an acceleration of the polymerization rate. Note that while the dispersion remains fluid up to full monomer conversion in case of PISA1, a gel than a solid were formed in case of PISA2 revealing the probable formation of cylinder-like structures.

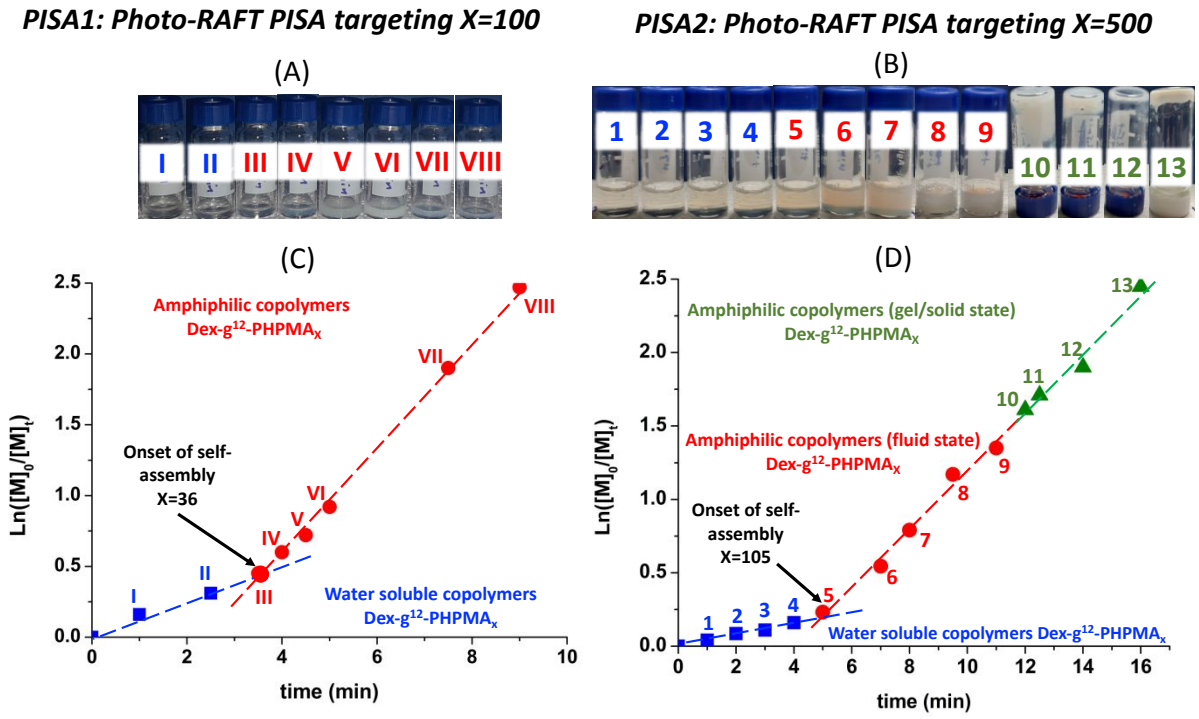

Figure 1. Photo-RAFT PISA of HPMA from $DexCTA_{12}$ using formulation at 10% w/w targeting: Dex-g^{12}-$PHPMA_{100}$ copolymers for PISA1 and Dex-g^{12}-$PHPMA_{500}$ copolymers for PISA2. A and B) visual appearance, and C and D) kinetic polymerization.

All aliquots sampled during PISA1 and PISA2 were lyophilized then analyzed by size exclusion chromatography (SEC) in DMSO/$NaNO_3$ at 70°C (**Figure S3**). The aliquots in the gel/solid state (samples: 10, 11, 12 and 13 of PISA2) were not characterized by SEC because copolymers formed some aggregates in the eluent, probably due to the occurrence of coupling reactions at high monomers conversion. As shown in **Table 1**, the number average molar masses ($\overline{M_n^{exp}}$) were relatively close to the theoretical ones ($\overline{M_n^{th}}$) and increased progressively with the monomer conversion (**Figure S3**), confirming the growth of the PHPMA grafts from dextran backbone during the photo-RAFT PISA. The relatively high dispersity (Đ > 1.4) may be attributed both to the relatively high dispersity of dextran and to the nonuniform distribution of CTA groups on the $DexCTA_{12}$ backbone leading to nonuniform distribution of PHPMA grafts on dextran backbone in the copolymer.

To get primary information on the nano-objects formed *in situ*, aliquots extracted in the fluid state (up to X=92 for PISA1 and 370 for PISA2) were first characterized by DLS to estimate the Z-average hydrodynamic radius (R_H) (**Table 1**). For PISA1, it was not possible to determine the size of the first intermediate structure at the onset of self-assembly time (X=36), probably due to the very small size of the nano-objects formed. However, when graft size reached 45 HPMA units after 30s of irradiation, one can observe formation of intermediate structures of 34nm radius that grow to 43nm at X=92. The size of such final nano-objects is in agreement with the one previously reported by us for ULV observed at X=100.[42] On the other hand, for PISA2, well-defined intermediate structures of close radii (R_H=40 to 45nm) were formed from the onset of self-assembly (X=105 to X=270). These sizes are close to ones observed for PISA1. One can wonder if the intermediate structures formed during PISA1 and PISA2 have a similar morphology. Sample extracted at 9.5min and 11min of irradiation (X=345 and 370 respectively) exhibit significant higher R_H revealing a probable morphology transition during the PISA process.

Table 1. Characteristics of intermediate structures withdrawn during the Photo-RAFT PISA of HPMA from $DexCTA_{12}$ at 10% w/w using formulation targeting: Dex-g^{12}-$PHPMA_{100}$ copolymers for PISA1 and Dex-g^{12}-$PHPMA_{500}$ copolymers for PISA2.

Entry	Aliquot	Time (min)	Conv (%)[a]	X[b]	$\overline{M_n^{exp}}$ [c] (kg/mol)	$\overline{M_n^{th}}$ [d] (kg/mol)	Đ[c]	R_H[e] (nm)	PDI[e]	R_{TEM} [f] (nm)	T_{CryoEM} [g] (nm)
PISA1	I	1.0	15	15	47	59	1.36	Hydrophilic copolymers			
	II	2.5	27	27	58	78	1.61				
	III	3.5	36	36	73	94	1.69	-	0.52	9.6 ± 1.4	-
	VI	4.0	45	45	92	109	1.72	34	0.46	26.3 ± 8.5	-
	V	4.5	51	51	110	123	1.78	33	0.34	37.7 ± 13	-
	VI	5.0	58	58	122	132	1.80	43	0.15	35.3 ± 15	13.4 ± 2
	VII	7.5	85	85	151	178	1.87	42	0.14	34.4 ± 10	17 ± 2.4
	VIII	9.0	92	92	170	190	1.90	43	0.17	35.8 ± 11	20 ± 2.6
PISA2	1	1.0	4.6	23	46	71	1.34	Hydrophilic copolymers			
	2	2.0	8.2	41	65	103	1.38				
	3	3.0	10 .4	52	100	122	1.44				
	4	4.0	14.9	74	200	161	1.50				
	5	5.0	21.0	105	230	213	1.59	40	0.15	63 ± 17	19 ± 2
	6	7.0	42.0	210	390	395	1.68	41	0.04	58 ± 8	32 ± 5
	7	8.0	54.7	270	440	500	1,72	45	0.04	61 ± 13	41 ± 8
	8	9.5	69.0	345	600	628	1.80	70	0.09	73 ± 20	45 ± 10
	9	11.0	74.0	370	800	672	1.90	99	0.20	103 ± 57	-

[a] Monomers conversion estimated by ^{1}H NMR analysis in DMSO-d_6 (Figure S1 and S2). [b] number average degree of polymerization of each PHPMA graft estimated by the following equation: $X = \frac{[HPMA]_0}{[CTA]_0} \times conv$. [c] Number average molecular weight and dispersity estimated by SEC analysis in DMSO/$NaNO_3$ at 70 °C. [d] Theoretical number average molecular weight estimated by the following equation: $\overline{M_n^{th}} = \frac{X \times M_{HPMA}}{X \times M_{HPMA} + M_{DexCTA}}$. [e] Hydrodynamic radius and polydispersity index obtained from DLS

analysis. [f] Average radius of 100 nano-objects from TEM images. [g] Average membrane thickness of 100 vesicles from cryoEM images.

TEM and cryoEM techniques were used to get deep information on such intermediate structures. **Figures 2 and 3** show images of aliquots during the PISA1 and PISA2 respectively. Additional images and statistical size analysis are available in **Figures S4−S7**. For PISA1 targeting a small grafts size (X=100), the first intermediate structures observed by TEM (**Figure 2**) at the onset of self-assembly (X=36) correspond to very small spherical micelles (S) in agreement with DLS analysis. Extending the grafts size to X= 45 induces a cooperative spheres-spheres fusion forming short worm-like micelles (WLM) composed of dimer or trimer micelles. We assume that spheres-spheres fusion is facilitated by the unreacted HPMA monomers that solvate the small PHPMA grafts.[3] Note that at this time, nano-objects were barely detected by cryoEM due to the small size of S and WLM. At X=51, TEM shows the coexistence of WLMs and their aggregates forming a spherical shape. On the other hand, cryoEM shows the presence of an incomplete bilayer in the shape of a 'jellyfish' (J) (hemispherical vesicle bearing WLM). This latter is suspected to be the key intermediate structure between WLMs and unilamellar vesicles (ULVs) as previously observed by Armes and coll.[3] for diblock copolymers. By adding only 7 HPMA monomer units in average for each graft (X=58), a complete closure of the 'jellyfish (J)' membrane has occurred leading to the formation of ULV. Finally, increasing the graft size to X= 85 and 92 induced the extension of the ULV membrane thickness (from 13 nm at X=58 to 20 nm at X=92) as judged by cryoEM. We assume that this extension of the membrane follows an inward pathway[23, 36, 47] as the average radius of vesicles remained close to one estimated at the appearance of the ULV at X=58 (**Table 1**). Although the mechanism proposed in **Figure 2c** was previously described for diblock copolymers, it provides strong evidence demonstrating that graft copolymers bearing short grafts length follow similar pathway to form vesicles in water.

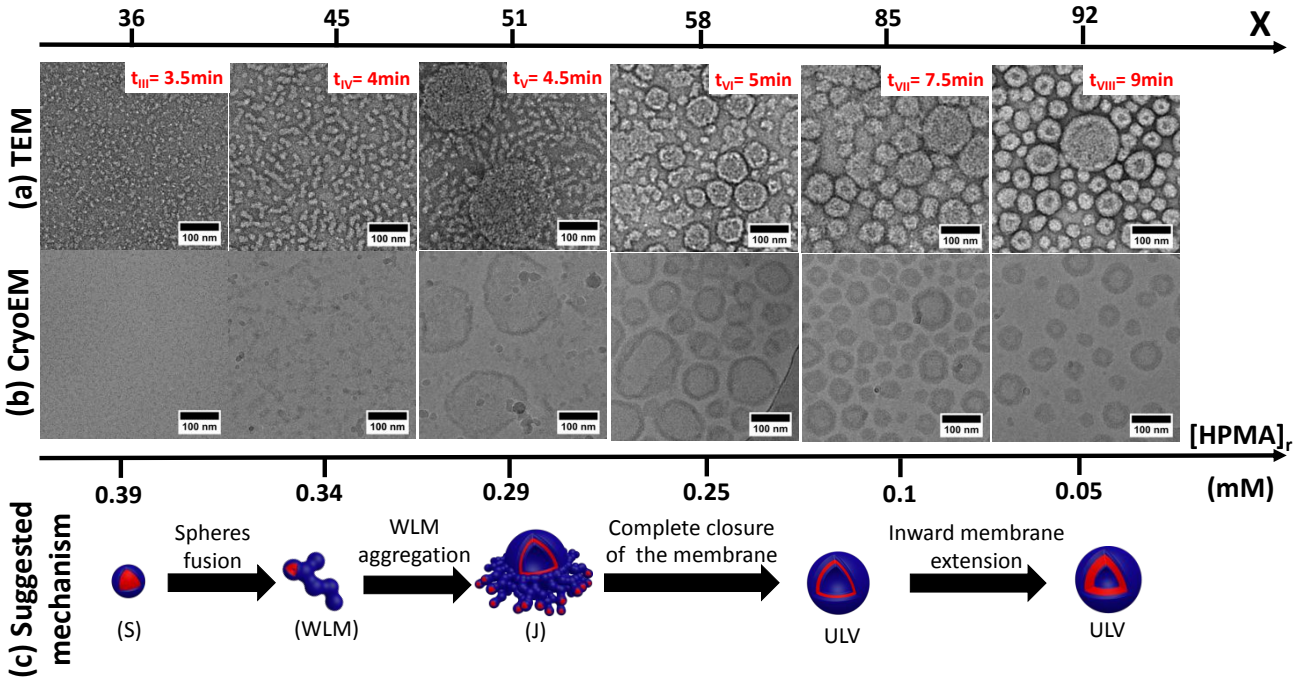

Figure 2. Intermediate structures withdrawn during the photo-RAFT PISA of HPMA from $DexCTA_{12}$ at 10% w/w targeting X=100 at full monomer conversion. a) TEM images, b) cryoEM images and c) suggested nano-objects evolution leading to the formation of ULV morphology. S: sphere, WLM: worm-like micelle, J: jellyfish, ULV: unilamellar vesicle. [HPMA]r is the residual HPMA concentration in the medium estimated from the monomers conversion.

In the case of PISA2 targeting longer grafts size (X=500), TEM images (**Figure 3**) reveal the formation of an unprecedented intermediate structure from the onset of copolymers self-assembly at X=105, composing of a clear membrane of 19nm surrounding multiple dark cores. We called this structure 'multi-compartment vesicles, MCV'.

It is well known that in TEM, samples can be stained with an aqueous solution of heavy metals in order to increase amplitude contrast in the image. In our case, samples were stained with 2% w/v aqueous solution of uranyl acetate that scatters electrons and appears as a dark area. Thus, the hydrophobic PHPMA grafts constitute the clear membrane while the dark areas are the aqueous domains. The multi-

compartment morphology is also clearly visible by cryoEM, which enables observation of nano-objects in their hydrated state. Note that the membrane appears dark in the cryoEM images since there is almost no amplitude contrast, because electrons interact very weakly with the light atoms of the specimen.

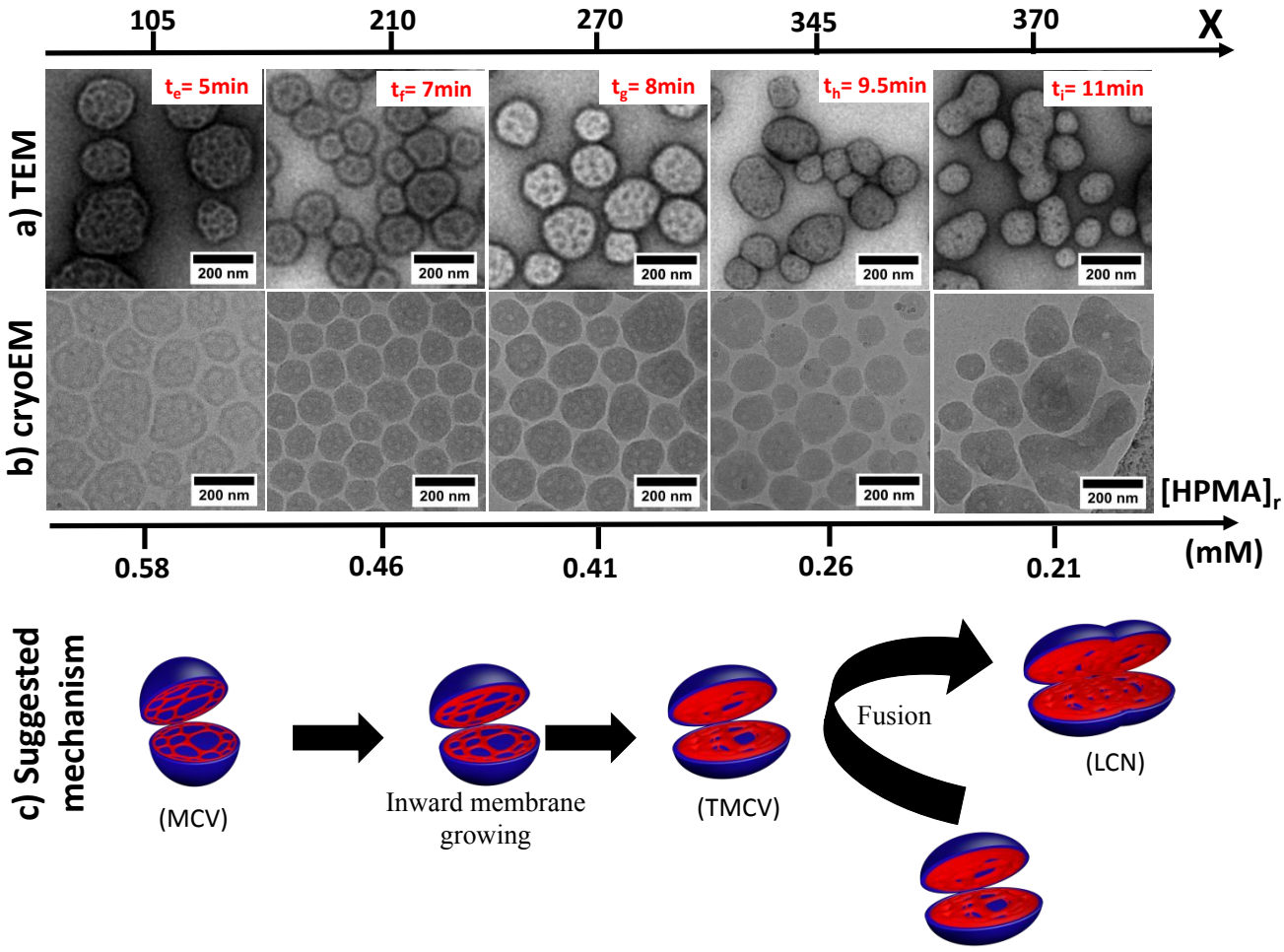

Figure 3. Intermediate structures withdrawn during the photo-RAFT PISA of HPMA from $DexCTA_{12}$ at 10% w/w targeting X=500 at full monomer conversion. a) TEM images, b) cryoEM images and c) suggested nano-objects evolution leading to the formation of LCNs. MCV: multi-compartment vesicle, TMCV: thick-membrane multi-compartment vesicle, LCN: large compound nano-object. $[HPMA]_r$ is the residual HPMA concentration in the medium estimated from the monomers conversion.

The multi-compartment morphology of the MCVs were visualized by the electron cryotomography (ECT) as judged by the **video 1** available in the supporting information. In ECT, a frozen-hydrated sample is progressively tilted using a goniometer to different angles relative to the electron beam by an increment of 2° up to negative 60° and to positive 60°. Thus, different images were collected producing a tilt-series images that were aligned and process to extract the 3D structure of the MCVs (**video 1**). The formation of this unprecedented morphology could be explained by the insolubility of dextran in HPMA (**Figure S8**). The high concentration of the local residual HPMA ($[HPMA]_r$, **Figure 3**), which enables solubilization of the PHPMA grafts during the PISA process, may induces a local phase separation with dextran leading to the formation of multiple aqueous domains in MCVs. To the best of our knowledge such intermediate structure has been never observed with others hydrophilic stabilizer such as poly(ethylene oxide),[35, 48] which is one of the most used polymers in PISA. This could be explained by the solubility of PEO in HPMA as judged in **Figure S8**.

Progressive extending of the grafts size to X= 210 and 270, induces growing of the membrane to 41nm without changing the shape and the size of the MCVs (**Table 1**). This suggests an inward growing of the membrane rather than an outward growing pathway. At X=345, MCVs become bigger with a larger membrane and barely noticeable aqueous cores. We called this intermediate morphology 'thick-membrane multi-compartment vesicle' (TMCV). Adding just 25 HPMA units to reach X=370 results in the generation of 'large compound nano-object' (LCN) as shown in TEM and cryoEM images. This structure appears as a superposing of several spheres, suggesting that it is formed according to a cooperative TMCV-TMCV fusion rather than an inward growing as suggested in the mechanism depicted in **Figure 3c.**

CONCLUSIONS.

In summary, Dex-g[12]-PHPMA$_X$ has been used as model to investigate the morphology evolution of graft copolymers during photo-RAFT PISA. Careful monitoring of the extracted samples at progressive monomers conversion revealed that copolymers of short grafts (X=100) formed ULV according to a mechanistic route similar to one reported for diblock copolymers. On the other hand, we have assumed that large compound nano-objects (LCNs) of cylindrical/spherical shapes, that were strangely formed when targeting longer grafts (X=500), resulted from an inter-fusion of ULVs. Our investigation revealed another mechanistic pathway and notably two interesting findings. Firstly, the absence of ULVs in all extracted samples in PISA targeting long graft size demonstrates that ULVs are not intermediate structures in the formation of LCNs. Secondly, the observation of novel nano-objects morphology composed of a membrane surrounding multiple hydrophilic cores, called multi-compartment vesicle (MCV), at early stage of self-assembly that were progressively grown and fused to form LCNs. The formation of this unprecedented structure was attributed to the local phase separation of dextran and PHMPA/HPMA leading to aqueous phase domains. The present investigation demonstrates that diagram of morphology, which is depicted from morphology at full monomer conversion, is not the best methodology to describe the mechanistic route of the nano-objects in PISA.

ASSOCIATED CONTENT.

*Supporting Information:

The Supporting Information is available free of charge on the ACS Publications website at DOI: Experimental protocols, characterization methods, NMR, SEC chromatograms, TEM and cryoEM images and statistical analysis.

AUTHOR INFORMATION.

Corresponding Author

*E-mail: khalid.ferji@univ-lorraine.fr

ORCID khalid FERJI: 0000-0003-3073-9722.

The authors declare no competing financial interest.

ACKNOWLEDGEMENTS.

The financial support from the French Agence Nationale de la Recherche (ANR JCJC, GlyNanEP No. 18-CE06-0002) is gratefully acknowledged. The authors acknowledge the CryoEM platform of I2BC, supported by iBiSA and by the French Infrastructure for Integrated Structural Biology (FRISBI) [ANR-10-INSB-05-05], and NanoImaging Core Facility of Pasteur Institute for acces to Glacios microscope. The authors thank O. Fabre for NMR characterization, A. Collar for SEC characterization, J.-C. Sivault for homemade UV lamp development. J-M. Winter for helping with tomograms recording.

REFERENCES.

1. Warren, N. J.; Armes, S. P., Polymerization-Induced Self-Assembly of Block Copolymer Nano-objects via RAFT Aqueous Dispersion Polymerization. *J. Am. Chem. Soc.* **2014,** *136* (29), 10174-10185.
2. D'Agosto, F.; Rieger, J.; Lansalot, M., RAFT-Mediated Polymerization-Induced Self-Assembly. *Angew. Chem.-Int. Edit.* **2020,** *59*, 8368–8392.
3. Blanazs, A.; Madsen, J.; Battaglia, G.; Ryan, A. J.; Armes, S. P., Mechanistic Insights for Block Copolymer Morphologies: How Do Worms Form Vesicles? *J. Am. Chem. Soc.* **2011,** *133* (41), 16581-16587.
4. Wan, W. M.; Pan, C. Y., One-pot synthesis of polymeric nanomaterials via RAFT dispersion polymerization induced self-assembly and re-organization. *Polym. Chem.* **2010,** *1* (9), 1475-1484.
5. Boissé, S.; Rieger, J.; Belal, K.; Di-Cicco, A.; Beaunier, P.; Li, M.-H.; Charleux, B., Amphiphilic block copolymer nano-fibers via RAFT-mediated polymerization in aqueous dispersed system. *Chem. Commun.* **2010,** *46* (11), 1950-1952.
6. Charleux, B.; Delaittre, G.; Rieger, J.; D'Agosto, F., Polymerization-Induced Self-Assembly: From Soluble Macromolecules to Block Copolymer Nano-Objects in One Step. *Macromolecules* **2012,** *45* (17), 6753-6765.

7. Sun, J.-T.; Hong, C.-Y.; Pan, C.-Y., Recent advances in RAFT dispersion polymerization for preparation of block copolymer aggregates. *Polym. Chem.* **2013,** *4* (4), 873-881.
8. Rieger, J., Guidelines for the Synthesis of Block Copolymer Particles of Various Morphologies by RAFT Dispersion Polymerization. *Macromol. Rapid Commun.* **2015,** *36* (16), 1458-1471.
9. Yeow, J.; Boyer, C., Photoinitiated Polymerization-Induced Self-Assembly (Photo-PISA): New Insights and Opportunities. *Adv. Sci.* **2017,** *4* (7), 1700137.
10. Burridge, K. M.; Wright, T. A.; Page, R. C.; Konkolewicz, D., Photochemistry for Well-Defined Polymers in Aqueous Media: From Fundamentals to Polymer Nanoparticles to Bioconjugates. *Macromol Rapid Commun* **2018,** *39* (12), e1800093.
11. Six, J. L.; Ferji, K., Polymerization induced self-assembly: an opportunity toward the self-assembly of polysaccharide-containing copolymers into high-order morphologies. *Polym. Chem.* **2019,** *10* (1), 45-53.
12. Penfold, N. J. W.; Yeow, J.; Boyer, C.; Armes, S. P., Emerging Trends in Polymerization-Induced Self-Assembly. *ACS Macro Lett.* **2019,** *8* (8), 1029-1054.
13. Pearce, S.; Perez-Mercader, J., PISA: construction of self-organized and self-assembled functional vesicular structures. *Polym. Chem.* **2021,** *12* (1), 29-49.
14. Semsarilar, M.; Abetz, V., Polymerizations by RAFT: Developments of the Technique and Its Application in the Synthesis of Tailored (Co)polymers. *Macromol. Chem. Phys.* **2021,** *222* (1), 2000311.
15. Khor, S. Y.; Truong, N. P.; Quinn, J. F.; Whittaker, M. R.; Davis, T. P., Polymerization-Induced Self-Assembly: The Effect of End Group and Initiator Concentration on Morphology of Nanoparticles Prepared via RAFT Aqueous Emulsion Polymerization. *ACS Macro Lett.* **2017,** *6* (9), 1013-1019.
16. Yan, X.; La Padula, V.; Favre-Bonte, S.; Bernard, J., Heptyl mannose decorated glyconanoparticles with tunable morphologies through polymerization induced self-assembly. Synthesis, functionalization and interactions with type 1 piliated E. coli. *European Polymer Journal* **2019,** *112*, 170-175.
17. Galanopoulo, P.; Dugas, P. Y.; Lansalot, M.; D'Agosto, F., Poly(ethylene glycol)-b-poly(vinyl acetate) block copolymer particles with various morphologies via RAFT/MADIX aqueous emulsion PISA. *Polym. Chem.* **2020,** *11* (23), 3922-3930.
18. Varlas, S.; Foster, J. C.; Georgiou, P. G.; Keogh, R.; Husband, J. T.; Williams, D. S.; O'Reilly, R. K., Tuning the membrane permeability of polymersome nanoreactors developed by aqueous emulsion polymerization-induced self-assembly. *Nanoscale* **2019,** *11* (26), 12643-12654.
19. Romero Castro, V. L.; Nomeir, B.; Arteni, A. A.; Ouldali, M.; Six, J.-L.; Ferji, K., Dextran-Coated Latex Nanoparticles via Photo-RAFT Mediated Polymerization Induced Self-Assembly. *Polymers* **2021,** *13* (23), 4064.
20. Varlas, S.; Keogh, R.; Xie, Y.; Horswell, S. L.; Foster, J. C.; O'Reilly, R. K., Polymerization-Induced Polymersome Fusion. *J. Am. Chem. Soc.* **2019,** *141* (51), 20234-20248.
21. Huang, L.; Ding, Y.; Ma, Y.; Wang, L.; Liu, Q.; Lu, X.; Cai, Y., Colloidal Stable PIC Vesicles and Lamellae Enabled by Wavelength-Orthogonal Disulfide Exchange and Polymerization-Induced Electrostatic Self-Assembly. *Macromolecules* **2019,** *52* (12), 4703-4712.
22. Wang, X.; Zhou, J.; Lv, X.; Zhang, B.; An, Z., Temperature-Induced Morphological Transitions of Poly(dimethylacrylamide)–Poly(diacetone acrylamide) Block Copolymer Lamellae Synthesized via Aqueous Polymerization-Induced Self-Assembly. *Macromolecules* **2017,** *50* (18), 7222-7232.

23. Czajka, A.; Armes, S. P., In situ SAXS studies of a prototypical RAFT aqueous dispersion polymerization formulation: monitoring the evolution in copolymer morphology during polymerization-induced self-assembly. *Chem. Sci.* **2020,** *11* (42), 11443-11454.
24. Blanazs, A.; Ryan, A. J.; Armes, S. P., Predictive Phase Diagrams for RAFT Aqueous Dispersion Polymerization: Effect of Block Copolymer Composition, Molecular Weight, and Copolymer Concentration. *Macromolecules* **2012,** *45* (12), 5099-5107.
25. Varlas, S.; Georgiou, P. G.; Bilalis, P.; Jones, J. R.; Hadjichristidis, N.; O'Reilly, R. K., Poly(sarcosine)-Based Nano-Objects with Multi-Protease Resistance by Aqueous Photoinitiated Polymerization-Induced Self-Assembly (Photo-PISA). *Biomacromolecules* **2018,** *19* (11), 4453-4462.
26. Wang, J.; Cao, M.; Zhou, P.; Wang, G., Exploration of a Living Anionic Polymerization Mechanism into Polymerization-Induced Self-Assembly and Site-Specific Stabilization of the Formed Nano-Objects. *Macromolecules* **2020,** *53* (8), 3157-3165.
27. Sarkar, J.; Xiao, L.; Jackson, A. W.; van Herk, A. M.; Goto, A., Synthesis of transition-metal-free and sulfur-free nanoparticles and nanocapsules via reversible complexation mediated polymerization (RCMP) and polymerization induced self-assembly (PISA). *Polym. Chem.* **2018,** *9* (39), 4900-4907.
28. Delaittre, G.; Dire, C.; Rieger, J.; Putaux, J.-L.; Charleux, B., Formation of polymer vesicles by simultaneous chain growth and self-assembly of amphiphilic block copolymers. *Chem. Commun.* **2009,** (20), 2887-2889.
29. Wan, W.-M.; Sun, X.-L.; Pan, C.-Y., Morphology Transition in RAFT Polymerization for Formation of Vesicular Morphologies in One Pot. *Macromolecules* **2009,** *42* (14), 4950-4952.
30. Wan, W.-M.; Hong, C.-Y.; Pan, C.-Y., One-pot synthesis of nanomaterials via RAFT polymerization induced self-assembly and morphology transition. *Chem. Commun.* **2009,** (39), 5883-5885.
31. Cai, W.; Wan, W.; Hong, C.; Huang, C.; Pan, C., Morphology transitions in RAFT polymerization. *Soft Matter* **2010,** *6* (21), 5554-5561.
32. Karagoz, B.; Boyer, C.; Davis, T. P., Simultaneous polymerization-induced self-assembly (PISA) and guest molecule encapsulation. *Macromol Rapid Commun* **2014,** *35* (4), 417-21.
33. Zhang, Y.; Wang, Z.; Matyjaszewski, K.; Pietrasik, J., Evolution of Morphology of POEGMA-b-PBzMA Nano-Objects Formed by PISA. *Macromol. Rapid Commun.* **2019,** *40* (2).
34. Yang, Y.; Zheng, J.; Man, S.; Sun, X.; An, Z., Synthesis of poly(ionic liquid)-based nano-objects with morphological transitions via RAFT polymerization-induced self-assembly in ethanol. *Polym. Chem.* **2018,** *9* (7), 824-827.
35. Warren, N. J.; Mykhaylyk, O. O.; Mahmood, D.; Ryan, A. J.; Armes, S. P., RAFT Aqueous Dispersion Polymerization Yields Poly(ethylene glycol)-Based Diblock Copolymer Nano-Objects with Predictable Single Phase Morphologies. *J. Am. Chem. Soc.* **2014,** *136* (3), 1023-1033.
36. Zhang, Q.; Zeng, R.; Zhang, Y.; Chen, Y.; Zhang, L.; Tan, J., Two Polymersome Evolution Pathways in One Polymerization-Induced Self-Assembly (PISA) System. *Macromolecules* **2020,** *53* (20), 8982-8991.
37. Feng, C.; Li, Y.; Yang, D.; Hu, J.; Zhang, X.; Huang, X., Well-defined graft copolymers: from controlled synthesis to multipurpose applications. *Chem. Soc. Rev.* **2011,** *40* (3), 1282-1295.
38. Sheiko, S. S.; Sumerlin, B. S.; Matyjaszewski, K., Cylindrical molecular brushes: Synthesis, characterization, and properties. *Prog. Polym. Sci.* **2008,** *33* (7), 759-785.
39. Kapishon, V.; Whitney, R. A.; Champagne, P.; Cunningham, M. F.; Neufeld, R. J., Polymerization Induced Self-Assembly of Alginate Based Amphiphilic Graft Copolymers Synthesized by Single Electron Transfer Living Radical Polymerization. *Biomacromolecules* **2015,** *16* (7), 2040-2048.

40. Ferji, K.; Venturini, P.; Cleymand, F.; Chassenieux, C.; Six, J.-L., In situ glyco-nanostructure formulation via photo-polymerization induced self-assembly. *Polym. Chem.* **2018,** *9* (21), 2868-2872.
41. Ikkene, D.; Arteni, A. A.; Ouldali, M.; Six, J.-L.; Ferji, K., Self-assembly of amphiphilic copolymers containing polysaccharide: PISA versus nanoprecipitation, and the temperature effect. *Polym. Chem.* **2020,** *11* (29), 4729-4740.
42. Ikkene, D.; Arteni, A. A.; Ouldali, M.; Francius, G.; Brûlet, A.; Six, J.-L.; Ferji, K., Direct Access to Polysaccharide-Based Vesicles with a Tunable Membrane Thickness in a Large Concentration Window via Polymerization-Induced Self-Assembly. *Biomacromolecules* **2021,** *22* (7), 3128-3137.
43. Israelachvili, J. N.; Mitchell, D. J.; Ninham, B. W., Theory of self-assembly of lipid bilayers and vesicles. *Biochimica et Biophysica Acta (BBA) - Biomembranes* **1977,** *470* (2), 185-201.
44. Ikkene, D.; Arteni, A. A.; Song, H.; Laroui, H.; Six, J. L.; Ferji, K., Synthesis of dextran-based chain transfer agent for RAFT-mediated polymerization and glyco-nanoobjects formulation. *Carbohydr. Polym.* **2020,** *234*, 115943.
45. Nomeir, B.; Fabre, O.; Ferji, K., Effect of Tertiary Amines on the Photoinduced Electron Transfer-Reversible Addition–Fragmentation Chain Transfer (PET-RAFT) Polymerization. *Macromolecules* **2019,** *52* (18), 6898-6903.
46. Kremer, J. R.; Mastronarde, D. N.; McIntosh, J. R., Computer Visualization of Three-Dimensional Image Data Using IMOD. *Journal of Structural Biology* **1996,** *116* (1), 71-76.
47. Warren, N. J.; Mykhaylyk, O. O.; Ryan, A. J.; Williams, M.; Doussineau, T.; Dugourd, P.; Antoine, R.; Portale, G.; Armes, S. P., Testing the Vesicular Morphology to Destruction: Birth and Death of Diblock Copolymer Vesicles Prepared via Polymerization-Induced Self-Assembly. *J. Am. Chem. Soc.* **2015,** *137* (5), 1929-1937.
48. Tan, J.; Sun, H.; Yu, M.; Sumerlin, B. S.; Zhang, L., Photo-PISA: shedding light on polymerization-induced self-assembly. *ACS Macro Lett.* **2015,** *4* (11), 1249-1253.